CHAPTER 5

HEAT TRANSFER ENHANCEMENT IN MICROCHANNEL HEAT SINKS USING MXENE-BASED NANOFLUIDS: A CFD APPROACH

Mohamad Nur Hidayat Mat[1], Nurizzatul Atikha Rahmat[1], Muhamad Mat Noor[1], Eliza M. Yusup[2], Muhammad Noor Afiq Muhammad Yazid[3], Nofrizalidris Darlis[4]

[1]Faculty of Mechanical and Automotive Engineering Technology, Universiti Malaysia Pahang Al-Sultan Abdullah, 26600 Pekan, Pahang, Malaysia

[2]Faculty of Mechanical & Manufacturing Engineering, Universiti Tun Hussein Onn, Parit Raja, 86400, Malaysia

[3]Faculty of Mechanical Engineering, Universiti Teknologi Malaysia, 81310, Johor Bahru, Johor, Malaysia

[4]Centre of Automotive & Powertrain Technology, Faculty of Engineering Technology, University Tun Hussein Onn Malaysia, Edu Hub Pagoh, 84600, Muar, Johor, Malaysia

ABSTRACT

As advancements in electronic technologies continue, the need for effective thermal management becomes increasingly vital. This research investigates the application of MXene-enhanced nanofluids at different volume concentrations in microchannel heat sinks to enhance cooling efficiency in electronic devices. Using numerical simulations based on a Eulerian multiphase framework, the study analyses the behavior and thermal properties of these nanofluids. Volume fractions ranging from 0.01% to 0.04% were assessed, and simulation results were cross validated with experimental data to ensure accuracy. At a Reynolds number of 300, a nanofluid concentration of 0.04 vol.% demonstrated a 20.1% decrease in thermal resistance when compared to water. Meanwhile, at Re 1000, the heat transfer coefficient improved by 29.4%. These outcomes indicate the promising potential of MXene-based nanofluids as advanced coolants for electronic heat sinks. The insights from this study are relevant across various electronic applications, such as power electronics, LEDs, and integrated circuits,

and may support the design of superior cooling solutions for domains like aerospace, high-performance computing, and automotive electronics.

Keywords: Heat transfer, microchannel heat sink, nanofluid, CFD

5.1 INTRODUCTION

The rapid development of electronic technology has driven the need for smaller, high-efficiency devices. Since Werner Jacobi's creation of the integrated circuit in 1949, electronic components have continuously evolved to become more compact and powerful. This trend aligns with Moore's Law, which states that the number of transistors on a chip doubles approximately every two years (Guarnieri, 2016). Although this advancement significantly improves computational capabilities, it also increases heat production at the component level—posing major challenges in managing heat. Without efficient thermal regulation, excessive heat can reduce device performance, compromise reliability, and shorten operational lifespan (Ortiz, Arévalo, Peña, & Jurado, 2024).

To tackle these thermal issues, microchannel heat sinks (MCHS) have emerged as promising solutions due to their excellent heat removal characteristics, large surface-area-to-volume ratios, and suitability for compact system integration (Gao, Hu, Yang, Liang, & Wu, 2022). However, the performance of MCHS is highly influenced by the type of coolant used. Traditional coolants such as water exhibit low thermal conductivity, motivating researchers to explore nanofluids, liquids embedded with nanoparticles, as potential alternatives to enhance thermal behavior (Ramesh, Sharma, & Rao, 2021).

Numerous investigations have demonstrated that nanofluids can substantially improve heat transfer performance. For instance, nanofluids containing ultra-fine particles (around 20 nm) have shown reductions in thermal resistance exceeding 37%, and enhancements in heat transfer coefficients of over 59%, due to their superior thermal conductivity and dispersion properties (Jasmee, Omar, Othaman, Masripan, & A. Hamid, 2021; Mebarek-Oudina & Chabani, 2022).

Experimental studies on Al_2O_3/water nanofluids with low particle loading (0.1–0.25%) have shown improvements in thermal performance of up to 33%. Furthermore, the use of hybrid nanofluids and modifications in Reynolds number have contributed to higher Nusselt numbers and better overall thermal performance (Hussein, Auda, Showard, & Dawood, 2025). Simulations have also indicated that trace levels of nanoparticles, such as BNNTs, can enhance both heat capacity and thermal conductivity. Optimized microchannel designs incorporating swirl flows and specific nanoparticle loadings have effectively

lowered thermal resistance and surface temperatures (An et al., 2023).

However, most existing studies focus on traditional nanoparticles like Al_2O_3, CuO, and diamond, with limited research addressing the potential of newer materials such as MXene nanoflakes. MXene, a two-dimensional material known for its excellent thermal conductivity and low viscosity, presents a promising alternative for use in nanofluid-based cooling systems (Fatima et al., 2021). Yet, its performance in microchannel heat sinks, particularly across a controlled range of volume fractions, remains insufficiently explored.

Considering these gaps, this study aims to investigate the thermal and flow performance of MXene-based nanofluids in microchannel heat sinks using a validated numerical approach. Specifically, the objective is to evaluate how varying nanofluid volume fractions (0.01–0.04 vol.%) influence thermal resistance, heat transfer coefficient, and overall cooling efficiency across different Reynolds numbers. The study employs a multiphase Eulerian model to capture inhomogeneous flow behaviours and validates simulation outcomes against experimental data to ensure reliability.

The novelty of this research lies in its systematic evaluation of MXene nanoflakes as a cooling medium in microchannel heat sinks under realistic operating conditions. By quantifying performance across multiple flow rates and nanofluid concentrations, the study contributes new insights into optimising thermal management strategies for advanced electronic systems. This work not only addresses the current lack of comprehensive data on MXene-based nanofluids but also supports the development of efficient, application-ready microchannel cooling solutions for high-performance computing, automotive, and aerospace applications.

5.2 METHODOLOGY

5.2.1 Geometry

The microchannel heat sink geometry was developed using Autodesk Inventor, comprising two distinct computational domains: a solid domain representing the heat sink material and a fluid domain representing the coolant flow. The designed model was then imported into ANSYS Fluent for numerical simulation. To optimise computational resources, only a single symmetric channel was selected for analysis, which sufficiently represents the thermal and flow behaviour of the complete microchannel structure.

As recommended in prior research, silicon was chosen as the construction

material due to its favourable thermal conductivity and widespread use in microelectronics cooling applications. (Ansari & Jeong, 2021). The design of the heat sink was tailored to meet the cooling requirements of modern microprocessor dies, which typically have a footprint of around 100 mm^2 (Tuckerman & Pease, 2005). Comparative studies have confirmed that silicon microchannel heat sinks offer better thermal performance than alternatives such as copper or aluminium under similar configurations (Sepehrnia & Rahmati, 2018).

The geometry of the microchannel heat sink as illustrated in Fig. 5.1, highlighting the inlet and outlet positions for fluid flow, as well as the length, width, and height of the entire sink (L_{sink}, W_{sink}, and H_{sink}, respectively). The model consists of multiple parallel fins and channels arranged to promote high surface area contact between the fluid and solid walls. A close-up view of the internal structure is provided in Fig. 5.1(b), which reveals the detailed dimensions of the microchannels and fins. Key geometric parameters include the channel width (W_{ch}), fin width (W_{fin}), base width (W_b), and fin height (H_{fin}), which is equal to the channel height (H_{ch}) in this configuration.

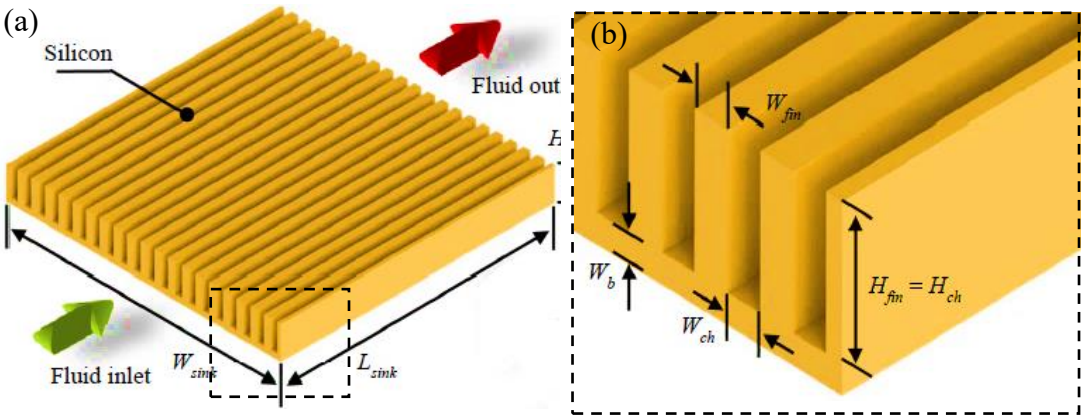

Fig. 5.1: (a) Overall view and (b) close-up view of the microchannel heat sink model (Ansari & Jeong, 2021)

This detailed geometric representation allows for accurate simulation of flow distribution and thermal interactions within the microchannel, forming the basis for evaluating heat transfer enhancement using nanofluids in subsequent analyses. The specific parameters and values used in this model are summarized in Table 5.1.

Table 5.1: Microchannel heat sink design parameter (Ansari & Jeong, 2021)

Design parameter	**Value (μm)**
Heat sink length (L_{sink})	10000
Heat sink width (W_{sink})	10000
Heat sink height (H_{sink})	1200
Fin height (H_{fin}) / Channel height (H_{ch})	1000
Fin width (W_{fin})	250
Channel width (W_{ch})	250
Base width (W_b)	200

5.2.2 Thermophysical Properties of Fluids

This work investigates the thermal and fluid flow behavior of microchannel heat sinks incorporating MXene-based nanofluids at varied concentrations. The nanofluid concentrations are incrementally set from 0.01% to 0.04% by 0.01% steps, with the MXene flake thickness consistently maintained at 1 nm. These values were chosen by referencing prior research that validated their thermal system stability and suitability (Abdollahi, Mohammed, Vanaki, & Sharma, 2018; Alfaryjat, Mohammed, Adam, Stanciu, & Dobrovicescu, 2018; Anasori & Gogotsi, 2019).

To ensure accurate modelling of thermal and flow characteristics, the thermophysical parameters of MXene nanofluids, namely specific heat, thermal conductivity, viscosity, and density, must be defined. These parameters are obtained either through established empirical formulas or from previously validated data available in the literature. For this study, the values were adopted from Das et al. (Das et al., 2020) who conducted investigations on MXene nanofluids applied in PV/T (photovoltaic/thermal) solar applications.

Table 5.2 summarizes the thermophysical properties for both pure water and the MXene nanofluids across all tested concentrations. When benchmarked against water, MXene-based nanofluids display marked improvements in thermal conductivity, along with increased viscosity and density. These changes influence convective heat transfer efficiency and fluid flow resistance. The observed properties are crucial in defining the overall performance in terms of heat transfer enhancement and pressure drop within the microchannel configuration.

Table 5.2: Thermophysical properties (Das et al., 2020)

Type of fluid	C_p (J/g.K)	k (W/m.K)	μ (mPa.s)	ρ (gm/cm³)
Typical water	4.017	0.536	0.756	0.997
MXene - 0.05 vol.%	2.275	0.570	2.650	1.046
MXene - 0.10 vol.%	2.324	0.665	2.700	1.048
MXene - 0.20 vol.%	2.413	0.710	2.730	1.050

5.2.3 Numerical Solver

In this study, numerical analysis was carried out using ANSYS Fluent 2022 R1 (Student Edition). The interaction between pressure and velocity fields was managed using the SIMPLE (Semi-Implicit Method for Pressure-Linked Equations) algorithm, which is particularly suitable for modelling steady and incompressible flow conditions. To discretize the governing equations, both first-order and second-order upwind schemes were employed for the momentum and energy equations, aligning with common CFD approaches referenced in the literature (Ali, Angelino, & Rona, 2021).

The convergence benchmarks were chosen based on established CFD standards to strike a balance between computational cost and solution precision. Residual limits were assigned as 1×10^{-6} for the continuity and momentum equations in all spatial directions (x, y, and z) to ensure solution stability. For the energy equation, a stricter criterion of 1×10^{-7} was adopted due to the sensitivity of thermal simulations, which require higher accuracy in temperature prediction.

These settings are consistent with previously published studies involving laminar flow in microchannels (Ajeeb, Oliveira, Martins, & Murshed, 2021; Shi, Li, Wei, & Gao, 2018), helping to minimize numerical error. The simulation was initiated using the standard initialization technique, which calculates initial conditions from all fluid zones, promoting uniformity across variables and enhancing convergence efficiency.

Boundary conditions were assigned as follows: a velocity inlet at the channel entrance and a pressure outlet at the exit. Details regarding the thermal and flow boundary conditions are provided in Section 2.5. To reduce computational cost while maintaining result accuracy, the simulation domain was restricted to half of a single microchannel, exploiting its geometrical symmetry.

The working fluid was modelled as a non-homogeneous mixture using a two-phase Eulerian approach. The primary phase consisted of pure water at 303 K, while the secondary phase was MXene nanoflakes ($Ti_3C_2T_x$) with a constant flake thickness of 1 nm. Simulations were conducted for four different nanofluid concentrations ranging from 0.01 vol.% to 0.04 vol.% to investigate the impact on heat transfer and fluid flow characteristics.

5.2.4 Flow Assumption and Governing Equations

The fluid flow and heat transfer in the microchannel heat sink are governed by the incompressible Navier–Stokes equations, which represent the conservation of mass, momentum, and energy. Given the low Mach number and small channel dimensions, the fluid is assumed incompressible and behaves as a continuous medium. These assumptions simplify the simulation without compromising accuracy.

The governing equations for Continuity equation (mass conservation):

$$\frac{\partial \rho}{\partial t} + \nabla \cdot (\rho v) = 0 \tag{5.1}$$

While for Momentum equation:

$$\frac{\partial (\rho v)}{\partial t} + \nabla \cdot (\rho v v) = -\nabla p + \nabla \cdot \tau + \rho g \tag{5.2}$$

And for Energy equation:

$$\frac{\partial (\rho e)}{\partial t} + \nabla \cdot (\rho v e) = -\nabla \cdot q + \nabla \cdot (\tau \cdot v) + \rho v \cdot g + \dot{q} \tag{5.3}$$

Here, ρ is fluid density, $\vec{u}$ is velocity, p is pressure, τ is the stress tensor, e is energy per unit mass, $\vec{q}$ is heat flux, and $\dot{q}$ is heat generation.

5.2.5 Boundary Conditions

To reduce computational effort, symmetry was applied across the mid-plane of the heat sink. The inlet was set as a velocity inlet, adjusted to achieve Reynolds numbers between 100 and 1000, with an inlet temperature of 30 °C for all fluid types. The outlet used a pressure outlet with 0 kPa gauge pressure. A no-slip condition was applied at all solid-fluid interfaces. A uniform heat flux of 6.6 W/cm^2 was imposed at the base of the heat sink to simulate heat input from electronic

components. Gravitational effects were included along the y-axis with an acceleration of 9.81 m/s^2.

5.2.6 Investigated Parameters

To evaluate the thermal and hydraulic performance of the microchannel heat sink (MCHS), several key parameters were analyzed. The Reynolds number (Re), which characterizes the flow regime, is calculated using:

$$Re = \frac{\rho V L}{\mu} \tag{5.4}$$

where V is the fluid velocity, L is the characteristic length (channel length), ρ is the fluid density, and μ is the dynamic viscosity. The pressure drop (Δp) across the channel is determined as:

$$\Delta p = P_{in} - P_{out} \tag{5.5}$$

P_{out} and P_{in} are the inlet and outlet pressures, respectively.

The temperature difference (ΔT) between inlet and outlet is given by:

$$\Delta T = T_{out} - T_{in} \tag{5.6}$$

To assess the heat removal efficiency, the thermal resistance (R_{th}) is calculated as:

$$R_{th} = \frac{T_{base} - T_{in}}{\dot{q}} \tag{5.7}$$

where T_{base} is the temperature at the base of the heat sink and $\dot{q}$ is the applied heat flux.

The average friction coefficient (C_f) is calculated using:

$$C_f = \frac{2 D_h \Delta p}{\rho {u_{in}}^2 L_{ch}} \tag{5.8}$$

where D_h is the hydraulic diameter, u_{in} is the inlet velocity, and L_{ch} is the channel length.

The convective heat transfer coefficient (h) for the nanofluid is calculated by:

$$h = \frac{\dot{q}}{T_{base} - T_m} \tag{5.9}$$

with the mean fluid temperature (T_m) defined as:

$$T_m = \frac{T_{in} + T_{out}}{2} \tag{5.10}$$

The pumping power (P_p) required to circulate the coolant through the channel is:

$$P_p = \Delta p Q \tag{5.11}$$

where Q is the volumetric flow rate. Finally, the Performance Evaluation Criteria (PEC), used to assess the overall performance of nanofluids relative to pure water, is given by:

$$PEC = \frac{h_{nf}/h_w}{\Delta p_{nf}/\Delta p_w} \tag{5.12}$$

where the subscript "nf" refers to the nanofluid and "w" to water. A PEC greater than 1 indicates improved thermal performance without a proportionally high-pressure penalty.

5.2.7 Mesh refinement study

To ensure mesh-independent results, a mesh sensitivity analysis was performed using three levels of grid resolution: coarse, medium, and fine. The analysis followed the Richardson extrapolation method, which estimates numerical error and predicts the asymptotic solution by comparing simulation outputs at different mesh densities. This approach helps identify the optimal mesh size that delivers accurate results without excessive computational cost. In this study, pressure drop and thermal resistance were selected as the key indicators to evaluate mesh convergence. As shown in Fig. 5.2, the pressure drop values for the fine, medium, and coarse meshes converge closely to the extrapolated solution. The relative extrapolation error for pressure drop was 0.36%, confirming that further mesh refinement would result in negligible accuracy improvement.

Similarly, Fig. 5.3 presents the thermal resistance behavior across the mesh refinements. The relative error compared to the extrapolated value was only 0.50%, again within acceptable limits. These results validate the selected mesh as sufficiently refined for the simulation. Based on this analysis, the fine mesh—consisting of approximately 799,324 elements with a representative element size of 22.46 μm and a cell length of 10.78 mm**,** was chosen for all subsequent numerical simulations. This ensures both numerical stability and reliable prediction of thermal and hydraulic performance in the microchannel heat sink.

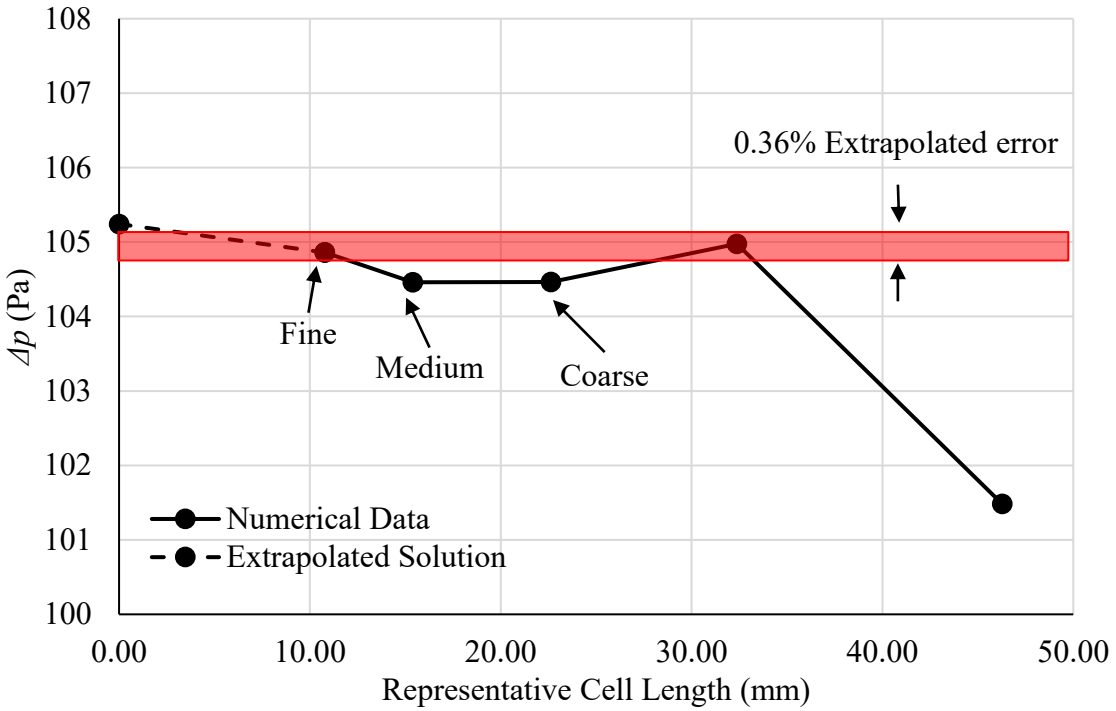

Fig. 5.2: Mesh refinement study for pressure drop

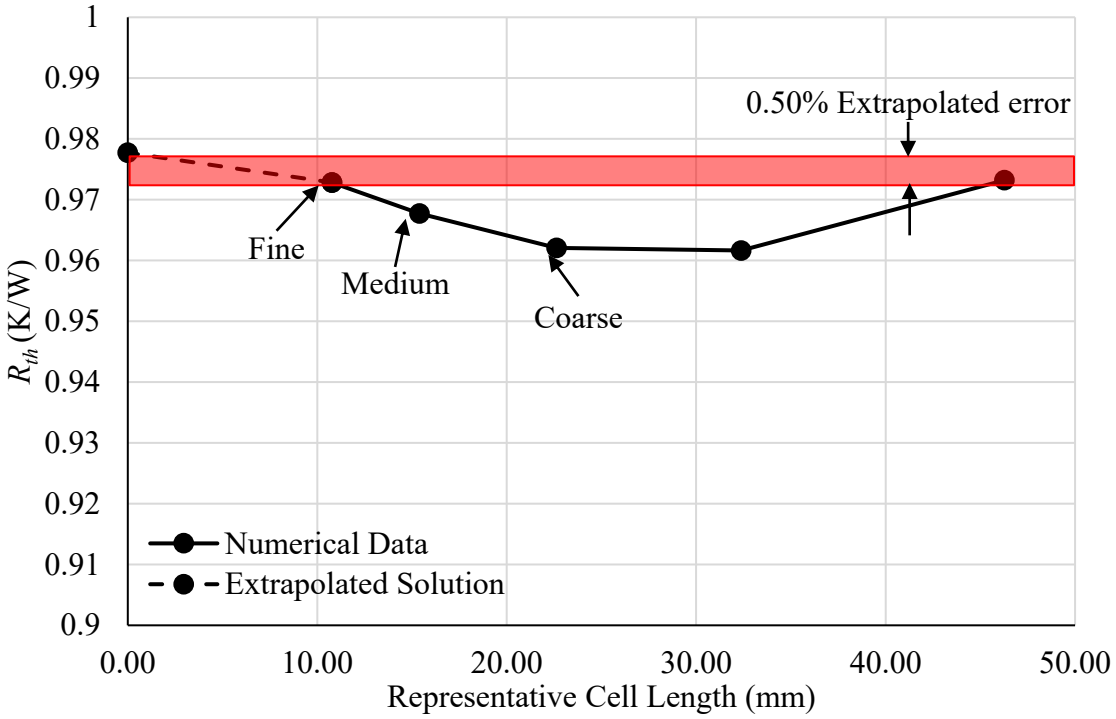

Fig. 5.3: Mesh refinement study for thermal resistance

5.2.8 Validation Study

To ensure the accuracy of the simulation model, a validation study was performed by comparing the present numerical results with established data from previous literature. The validation was conducted using water as the working fluid, which is consistent with the baseline condition used in the cited studies. This approach

ensures similarity in physical properties and boundary conditions, allowing for a reliable comparison based on a similarity-based validation method (Cooke, Steinke, Wallraven, & Bülthoff, 2005).

The first validation, presented in Fig. 5.4**,** compares the predicted apparent friction coefficient C_f against the results reported by Jia et al. (Li, Xia, Ma, Jia, & Wang, 2016) across a range of Reynolds numbers. The figure shows a consistent trend between both data sets, with minimal deviation at lower Reynolds numbers. The lowest relative error is observed at Re=150Re = 150 with just 0.5%, while the highest discrepancy of 16.6% occurs at Re=650Re = 650. Overall, the close alignment at lower Re confirms the model's capability to predict friction behavior accurately under laminar flow conditions.

The second validation, shown in Fig. 5.5**,** evaluates the pressure drop (Δp) by comparing current simulation results with those from Prajapati et al. (Prajapati, 2019). A strong agreement is observed between both datasets, especially at lower Reynolds numbers. The relative error ranges from 0.4% at Re=150Re = 150 to a maximum of 15.2% at Re=650Re = 650. These results indicate that the numerical model reliably captures pressure characteristics within the tested Re range. In summary, the validation results demonstrate good agreement with previous research, particularly in the low Reynolds number regime, supporting the reliability of the selected mesh and boundary conditions for the current study.

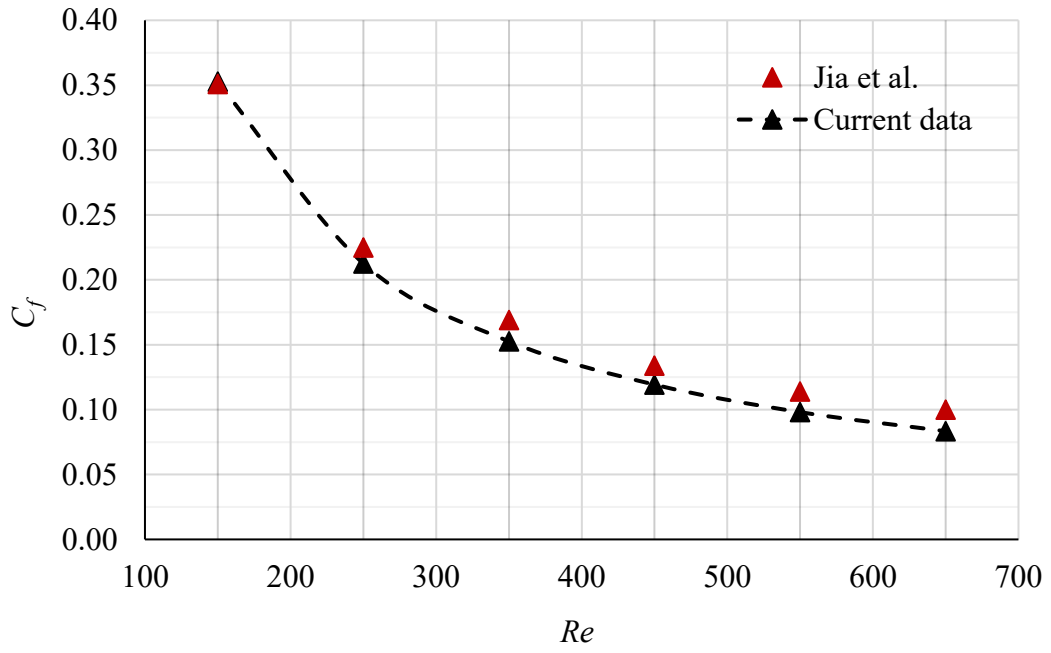

Fig. 5.4: Validation of apparent friction coefficient with previous work (Li et al., 2016)

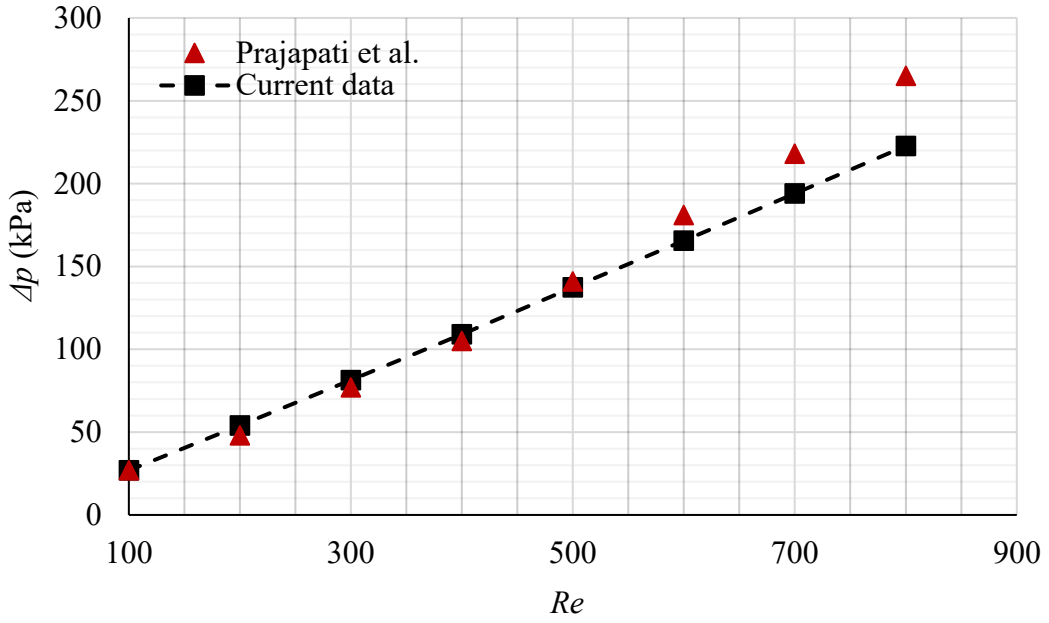

Fig. 5.5: Validation of pressure drop (Prajapati, 2019)

5.3 RESULTS AND DISCUSSION

5.3.1 Flow Pattern of Pressure Distribution

Fig. 5.6 presents the pressure contour plots for different concentrations of MXene nanoflakes in water, ranging from pure water to 0.04 vol.%. These plots illustrate the pressure variation along the microchannel length and highlight the effect of increasing nanoparticle concentration on flow resistance. Since the outlet boundary is set to atmospheric pressure (0 Pa), all cases show a consistent pressure value at the channel exit. However, the inlet pressure increases noticeably with higher MXene concentrations. This is attributed to the enhanced viscosity caused by the presence of nanoflakes, which increases internal friction and flow resistance within the channel. Among all the tested cases, the 0.04 vol.% nanofluid exhibits the highest inlet pressure, reaching approximately 88 Pa. In contrast, pure water shows the lowest pressure at the same flow condition. The increasing pressure gradient along the channel with higher concentrations indicates that more pumping power is required to maintain flow, which is critical for practical heat sink design. In summary, pressure distribution analysis confirms that MXene concentration has a direct impact on the hydrodynamic behaviour of the nanofluid. Understanding this relationship is essential for optimising both thermal and hydraulic performance in microchannel cooling systems.

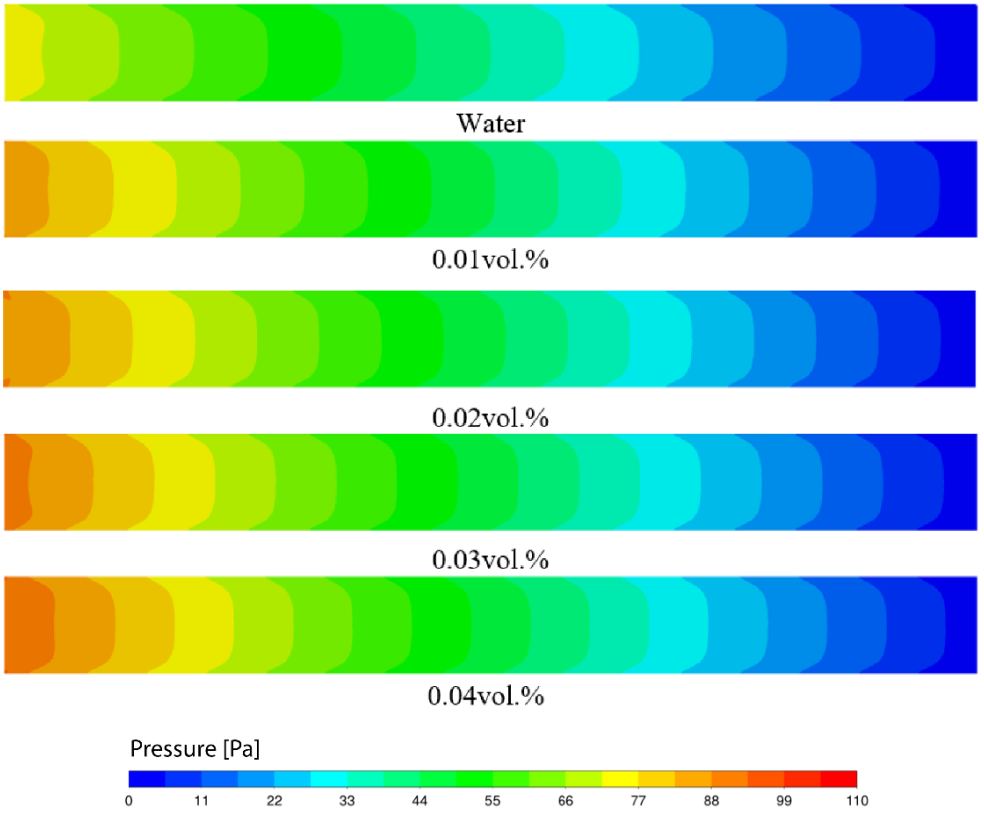

Fig. 5.6: Pressure contour plot of different concentrations

5.3.2 Flow Pattern Velocity Distribution

Fig. 5.7 illustrates the velocity contour plots of the working fluid for pure water and MXene nanofluids at various concentrations (0.01–0.04 vol.%). These plots reveal the velocity distribution along the microchannel and the influence of nanoparticle concentration on flow behaviour. As seen in the contours, the maximum velocity occurs at the centre of the channel, consistent with laminar flow profiles. For pure water, the peak velocity reaches approximately 0.074 m/s. However, with the addition of MXene nanoflakes, the velocity decreases to around 0.059 m/s across all concentrations, representing a reduction of approximately 20.27%. This drop is primarily due to the increased viscosity of the nanofluids, which adds resistance to the flow. Interestingly, despite the variation in concentration, the velocity contours for 0.01 to 0.04 vol.% show only slight differences. This indicates that while MXene inclusion significantly alters the flow field compared to water, the incremental increases in concentration do not markedly affect the velocity due to relatively minor changes in viscosity beyond the initial addition. In summary, the presence of MXene nanoflakes modifies the velocity distribution within the microchannel. Although the reduction in velocity may seem counterintuitive, it can enhance thermal performance by improving energy transport mechanisms within the fluid. These findings highlight the delicate balance between flow resistance and thermal enhancement in nanofluid

applications.

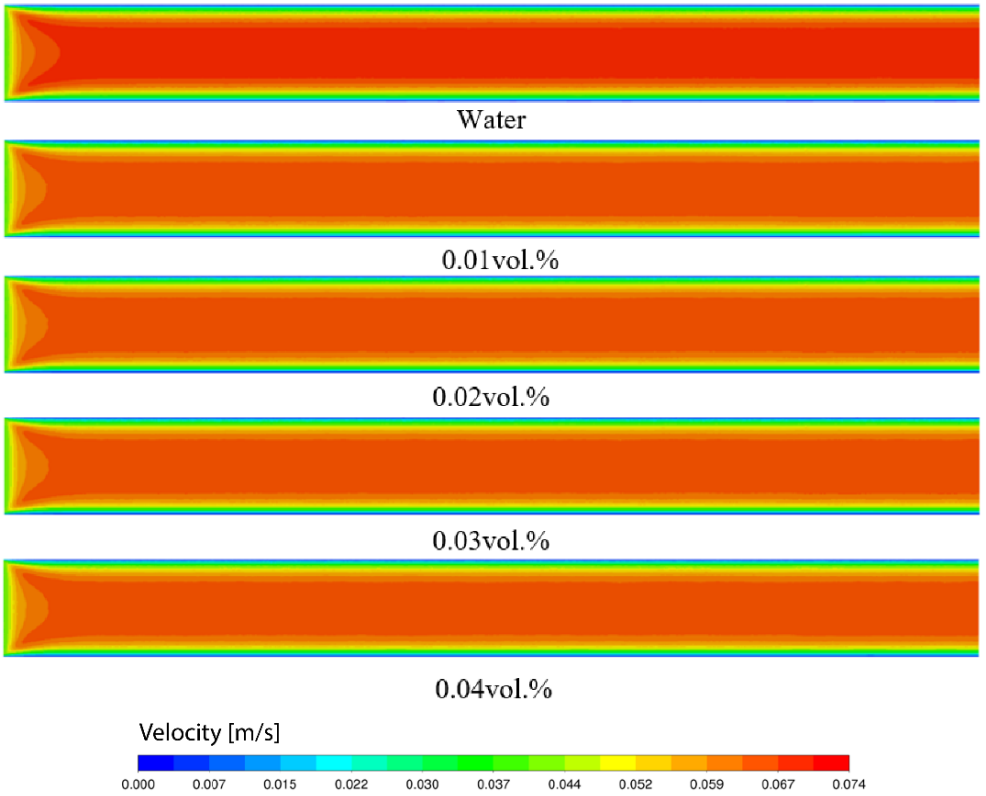

Fig. 5.7: Velocity contour plot of different concentrations

5.3.3 Flow Pattern of Temperature Distribution

Fig. 5.8 presents the temperature contour plots for pure water and MXene nanofluids at concentrations ranging from 0.01 vol.% to 0.04 vol.%. These contours illustrate how temperature evolves along the length of the microchannel under constant heat flux conditions. The results show a clear trend: increasing the concentration of MXene nanoflakes reduces the outlet temperature of the coolant. Pure water exhibits the highest base temperature at the outlet, approximately 312 K, whereas the 0.04 vol.% nanofluid shows the lowest at around 309.5 K, indicating a 0.8% reduction**.** Similarly, the coolant temperature at the outlet drops by about 0.5% when comparing water to the 0.04 vol.% nanofluid. This behaviour can be attributed to the enhanced thermal conductivity of nanofluids. As MXene concentration increases, more nanoparticles actively participate in heat transport, enabling more efficient energy extraction from the heated base. As a result, the fluid leaves the channel at a lower temperature, indicating improved thermal performance. These findings are consistent with previous studies that report similar reductions in base temperature with higher nanoparticle loadings (Al-Rashed et al., 2019). The trend underscores the importance of nanofluid concentration as a key parameter in optimising cooling performance within microchannel heat sinks.

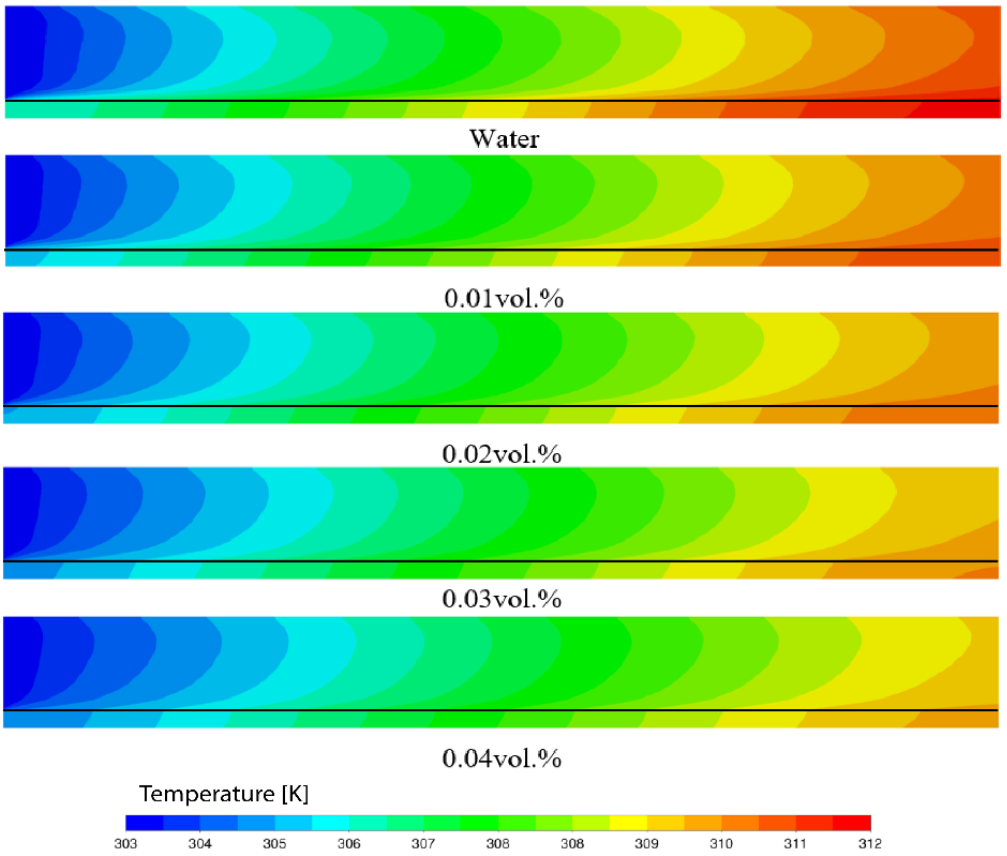

Fig. 5.8: Temperature contour plot of different concentrations

5.3.4 Thermophysical Behavior of Pressure Distribution

Fig. 5.9 shows the pressure variation along the microchannel length, plotted as a function of relative distance (x/Lx/L) for pure water and MXene nanofluids with concentrations from 0.01% to 0.04%. A clear linear decrease in pressure is observed across all cases, consistent with laminar flow in confined channels where frictional losses dominate. Among the fluids tested, pure water demonstrates the lowest inlet pressure at approximately 72.89 Pa, while the 0.04 vol.% nanofluid shows the highest, reaching 90.91 Pa - a 24% increase. Each incremental rise in concentration leads to a modest increase in pressure, typically around 2.4%, indicating that the addition of MXene nanoflakes introduces slight but consistent increases in flow resistance. This rise in pressure can be attributed to the increased viscosity of the nanofluids and potential nanoparticle interaction with the channel walls, which may influence near-wall flow behaviour. As the nanoflake concentration increases, the enhanced interfacial friction may alter the boundary layer and overall pressure profile. The nearly parallel slopes of the pressure curves for all concentrations suggest that while the overall pressure drop remains similar, the absolute pressure level rises with nanoparticle content. This observation highlights the subtle but important role of nanoflakes in shaping fluid

dynamics and underscores the importance of accounting for nanoscale effects in the design of high-performance microchannel systems.

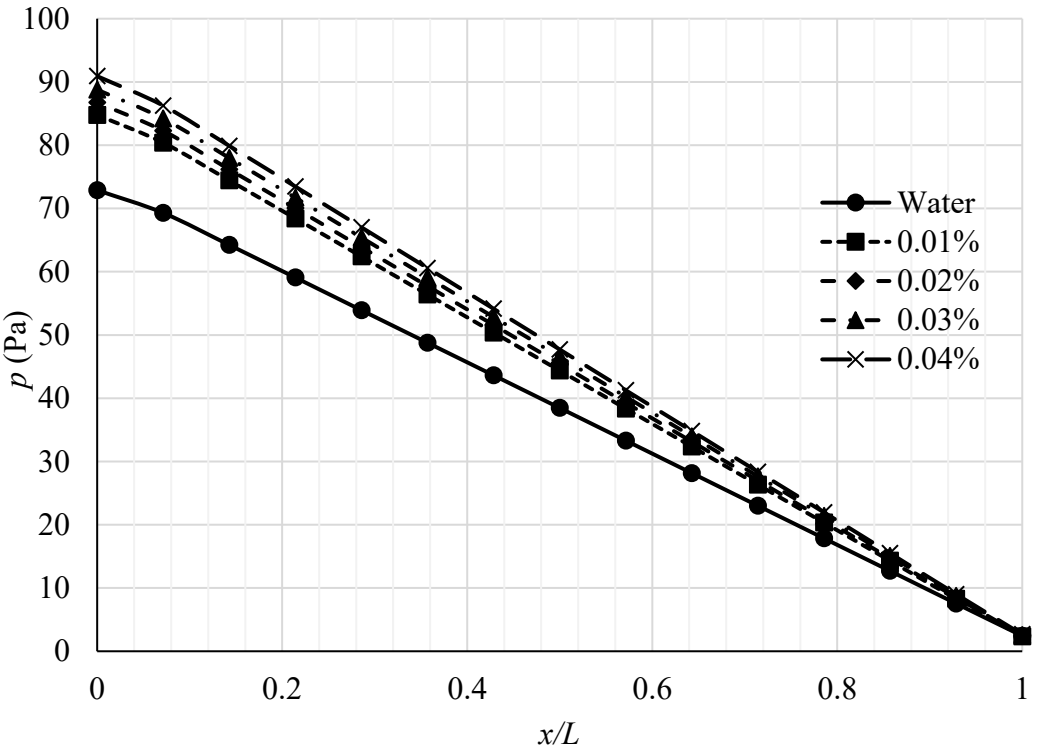

Fig. 5.9: Pressure vs. x/L in the fluid domain

5.3.5 Thermophysical Behavior of Temperature Distribution

Fig. 5.10 shows the temperature distribution along the channel length (x/L) for pure water and MXene nanofluids at varying concentrations. As expected, the fluid temperature increases progressively from the inlet to the outlet due to the applied heat flux at the microchannel base. Pure water exhibits the highest outlet temperature at approximately 310.7 K, while the lowest outlet temperature of 309.4 K is recorded for the 0.04 vol.% MXene nanofluid—representing a temperature reduction of about 0.41%. This indicates that higher nanoparticle concentrations enhance heat extraction from the channel walls, resulting in cooler fluid at the outlet. The total temperature rise from inlet to outlet also varies with concentration: 2.54% for water, and slightly lower increments of 2.43%, 2.32%, 2.22%, and 2.12% for 0.01% to 0.04% MXene nanofluids, respectively. This consistent trend confirms that adding MXene nanoflakes improves thermal performance by increasing thermal conductivity and facilitating more efficient heat transfer. These results align with prior studies that observed greater temperature reductions with increasing nanoparticle content. For instance, a 0.05 vol.% concentration was previously reported to reduce outlet temperature by up to 9.2 °C (Sarvar-Ardeh, Rafee, & Rashidi, 2021). In conclusion, the use of MXene nanofluids effectively enhances convective heat transfer in microchannel

heat sinks, making them suitable for high-efficiency cooling applications.

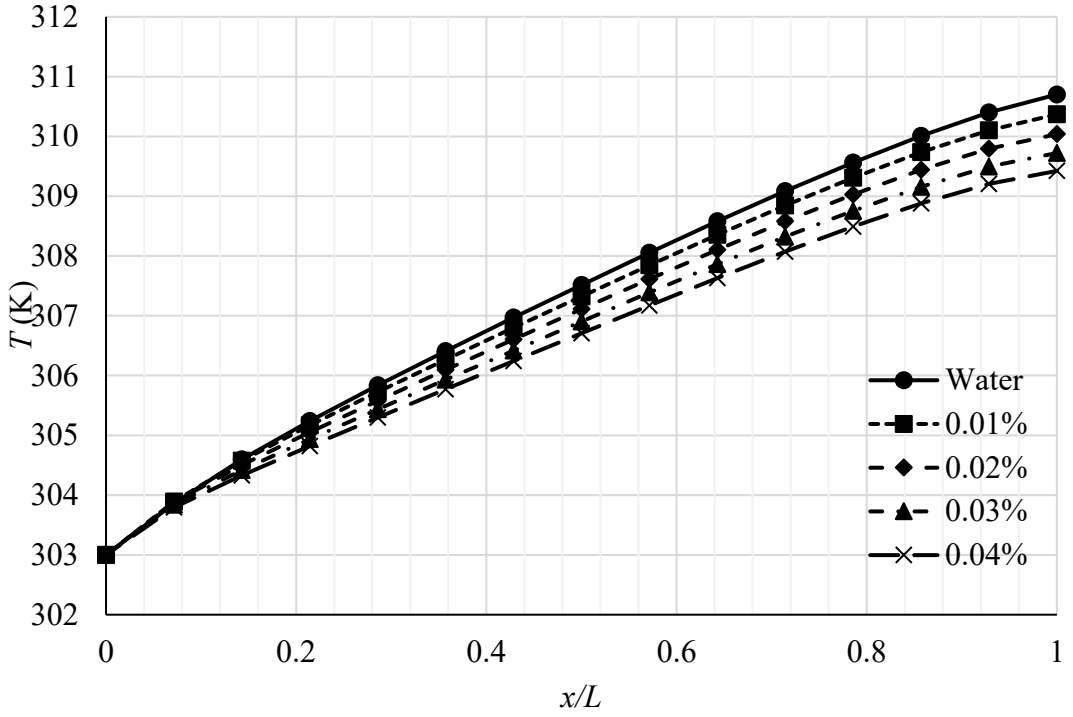

Fig. 5.10: Temperature vs. x/L in the fluid domain

5.4 ACKNOWLEDGEMENT

The authors would like to express their sincere gratitude to Universiti Malaysia Pahang Al-Sultan Abdullah (UMPSA) for the financial and technical support provided throughout this study. Special thanks are also extended to the co-author(s) for their valuable contributions, insightful discussions, and continuous collaboration that significantly enriched the quality of this work.

5.6 REFERENCE

Abdollahi, A., Mohammed, H. A., Vanaki, S. M., & Sharma, R. N. (2018). Numerical investigation of fluid flow and heat transfer of nanofluids in microchannel with longitudinal fins. *Ain Shams Engineering Journal, 9*(4), 3411-3418.

Ajeeb, W., Oliveira, M. S., Martins, N., & Murshed, S. S. (2021). Forced convection heat transfer of non-Newtonian MWCNTs nanofluids in microchannels under laminar flow. *International Communications in Heat and Mass Transfer, 127*, 105495.

Al-Rashed, A. A., Shahsavar, A., Rasooli, O., Moghimi, M., Karimipour, A., & Tran, M. D. (2019). Numerical assessment into the hydrothermal and entropy generation characteristics of biological water-silver nano-fluid in a wavy walled microchannel heat sink. *International Communications in Heat and Mass Transfer, 104*, 118-126.

Alfaryjat, A., Mohammed, H., Adam, N. M., Stanciu, D., & Dobrovicescu, A. (2018). Numerical investigation of heat transfer enhancement using various nanofluids in hexagonal microchannel heat sink. *Thermal Science and Engineering Progress, 5*, 252-262.

Ali, A. M., Angelino, M., & Rona, A. (2021). Numerical analysis on the thermal performance of microchannel heat sinks with Al2O3 nanofluid and various fins. *Applied Thermal Engineering, 198*, 117458.

An, L., Yu, Y., Cai, Q., Mateti, S., Li, L. H., & Chen, Y. I. (2023). Hexagonal boron nitride nanosheets: preparation, heat transport property and application as thermally conductive fillers. *Progress in Materials Science, 138*, 101154.

Anasori, B., & Gogotsi, Û. G. (2019). *2D metal carbides and nitrides (MXenes)* (Vol. 2549): Springer.

Ansari, D., & Jeong, J. H. (2021). A silicon-diamond microchannel heat sink for die-level hotspot thermal management. *Applied Thermal Engineering, 194*, 117131.

Cooke, T., Steinke, F., Wallraven, C., & Bülthoff, H. H. (2005). *A similarity-based approach to perceptual feature validation.* Paper presented at the Proceedings of the 2nd Symposium on Applied Perception in Graphics and Visualization.

Das, L., Habib, K., Saidur, R., Aslfattahi, N., Yahya, S. M., & Rubbi, F. (2020). Improved thermophysical properties and energy efficiency of aqueous ionic liquid/mxene nanofluid in a hybrid pv/t solar system. *Nanomaterials, 10*(7), 1372.

Fatima, U., Tahir, M. B., Sagir, M., Fatima, N., Nawaz, T., Bhatti, M. P., & Ashraf, N. (2021). Two-dimensional materials and synthesis, energy storage, utilization, and conversion applications of two-dimensional MXene materials. *International Journal of Energy Research, 45*(7), 9878-9894.

Gao, J., Hu, Z., Yang, Q., Liang, X., & Wu, H. (2022). Fluid flow and heat transfer in microchannel heat sinks: Modelling review and recent progress. *Thermal Science and Engineering Progress, 29*, 101203.

Guarnieri, M. (2016). The unreasonable accuracy of Moore's Law [Historical]. *IEEE Industrial Electronics Magazine, 10*(1), 40-43.

Hussein, A. A., Auda, A. C., Showard, A. F., & Dawood, H. (2025). Heat transfer enhancement by utilizing Al2O3-Water nanofluid in a coiled agitated vessel. *Case Studies in Thermal Engineering, 66*, 105740.

Jasmee, S., Omar, G., Othaman, S. S. C., Masripan, N. A., & A. Hamid, H. (2021). Interface thermal resistance and thermal conductivity of polymer composites at different types, shapes, and sizes of fillers: A review. *Polymer Composites, 42*(6), 2629-2652.

Li, Y., Xia, G., Ma, D., Jia, Y., & Wang, J. (2016). Characteristics of laminar flow and heat transfer in microchannel heat sink with triangular cavities and rectangular ribs. *International Journal of Heat and Mass Transfer, 98*, 17-28.

Mebarek-Oudina, F., & Chabani, I. (2022). Review on nano-fluids applications and heat transfer enhancement techniques in different enclosures. *Journal of Nanofluids, 11*(2), 155-168.

Ortiz, Y., Arévalo, P., Peña, D., & Jurado, F. (2024). Recent advances in thermal management strategies for lithium-ion batteries: a comprehensive review. *Batteries, 10*(3), 83.

Prajapati, Y. K. (2019). Influence of fin height on heat transfer and fluid flow characteristics of rectangular microchannel heat sink. *International Journal of Heat and Mass Transfer, 137*, 1041-1052.

Ramesh, K. N., Sharma, T. K., & Rao, G. A. P. (2021). Latest advancements in heat transfer enhancement in the micro-channel heat sinks: a review. *Archives of Computational Methods in Engineering, 28*, 3135-3165.

Sarvar-Ardeh, S., Rafee, R., & Rashidi, S. (2021). Hybrid nanofluids with temperature-dependent properties for use in double-layered microchannel heat sink; hydrothermal investigation. *Journal of the Taiwan Institute of Chemical Engineers, 124*, 53-62.

Sepehrnia, M., & Rahmati, A. (2018). Numerical investigating the gas slip flow in the microchannel heat sink using different materials. *Challenges in Nano and Micro Scale Science and Technology, 6*(Special Issue), 44-50.

Shi, X., Li, S., Wei, Y., & Gao, J. (2018). Numerical investigation of laminar convective heat transfer and pressure drop of water-based Al2O3 nanofluids in a microchannel. *International Communications in Heat and Mass Transfer, 90*, 111-120.

Tuckerman, D. B., & Pease, R. F. W. (2005). High-performance heat sinking for VLSI. *IEEE Electron device letters, 2*(5), 126-129.